JACS
JOURNAL OF THE AMERICAN CHEMICAL SOCIETY
pubs.acs.org/JACS
Article

$n\rightarrow\pi^*$ Interactions Modulate the Disulfide Reduction Potential of Epidithiodiketopiperazines

Henry R. Kilgore,[†] Chase R. Olsson,[†] Kyan A. D'Angelo, Mohammad Movassaghi,* and Ronald T. Raines*

Cite This: *J. Am. Chem. Soc.* 2020, 142, 15107−15115
Read Online
ACCESS | Metrics & More | Article Recommendations | Supporting Information

ABSTRACT: Epithiodiketopiperazines (ETPs) are a structurally complex class of fungal natural products with potent anticancer activity. In ETPs, the diketopiperazine ring is spanned by a disulfide bond that is constrained in a high-energy eclipsed conformation. We employed computational, synthetic, and spectroscopic methods to investigate the physicochemical attributes of this atypical disulfide bond. We find that the disulfide bond is stabilized by two $n\rightarrow\pi^*$ interactions, each with large energies (3−5 kcal/mol). The $n\rightarrow\pi^*$ interactions in ETPs make disulfide reduction much more difficult, endowing stability in physiological environments in a manner that could impact their biological activity. These data reveal a previously unappreciated means to stabilize a disulfide bond and highlight the utility of the $n\rightarrow\pi^*$ interaction in molecular design.

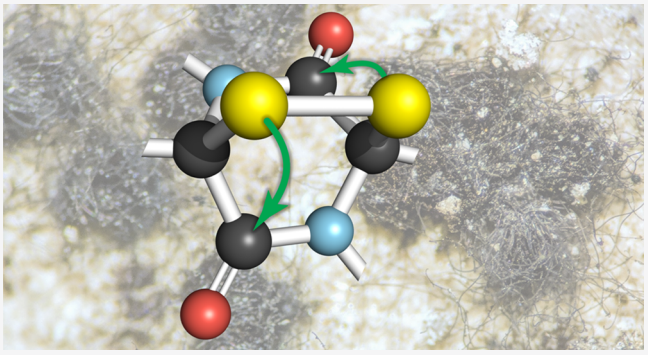

INTRODUCTION

Organisms are engaged in an incessant race to evolve strategies against selective pressures.[1] Among fungi such as *Chaetomium* spp., the strategy to avoid predation or abate competition is manifested in the form of natural products such as epithiodiketopiperazines (ETPs).[2] ETPs comprise a structurally diverse and biologically active family of fungal alkaloids characterized by a disulfide (or polysulfide) that bridges a 2,5-diketopiperazine (DKP) (Figure 1A).[3,4] Combination of the unique and challenging molecular architecture of ETPs[3,4] and their potent biological activity[2] has captured the attention of scientists across a wide range of disciplines.[5−7]

Structure−activity relationships have revealed that the activity of ETPs is dependent upon reduction of the epidisulfide bond (Figure 1B) that spans the DKP ring.[4,5,8] Unlike those in proteins, the disulfide bonds in ETPs are locked in an eclipsed conformation (Figure 1C).[9] In dimethyl disulfide, a prototypical disulfide, values for the C−S−S−C dihedral angle near 0° correspond to ∼10 kcal/mol of strain energy (Figure 1C).[10] We reasoned that a compensatory force must exist within ETPs to ameliorate the instability imposed by the eclipsed conformation.

Here, we report on the physicochemical underpinnings of the disulfide bond of ETPs. We began by considering ETP natural products and used quantum mechanical methods to search for the origin of the stability of the disulfide bond. These investigations revealed that $n\rightarrow\pi^*$ interactions[11] that arise from the overlap of the p-type lone pairs of the sulfur atoms with the π^* orbitals of the amide carbonyl groups (Figure 1D) are an integral component of ETP alkaloids. We then synthesized and structurally analyzed a series of C4-substituted bisprolyl-ETPs that were designed to manipulate the energetics of the $n\rightarrow\pi^*$ interaction, and we measured the reduction potential of these synthetic ETPs. We find that C4 substitution perturbs the $n\rightarrow\pi^*$ interaction and correlated parameters, including the disulfide reduction potential. Our data support a role for $n\rightarrow\pi^*$ interactions in tuning the reduction potential of ETPs and thus their biological activities.

RESULTS AND DISCUSSION

$n\rightarrow\pi^*$ Interactions in ETPs. To investigate the chemical forces that stabilize the strained disulfide bridge, we examined a structurally diverse catalog of natural ETPs with known crystal structures. Untethered disulfide bonds prefer a C−S−S−C dihedral angle near $|\theta| = 90°$ (Figure 1C).[12] In ETPs, the value of $|\theta|$ is <20° (Figure 2A), which is near an energy maximum (Figure 1C). We suspected that the strength of the two $n\rightarrow\pi^*$ interactions in an ETP could compensate for the strain energy of its eclipsed disulfide bond and that evidence

Received: June 19, 2020
Published: July 23, 2020

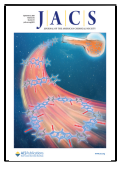

ACS Publications
© 2020 American Chemical Society

https://dx.doi.org/10.1021/jacs.0c06477
J. Am. Chem. Soc. 2020, 142, 15107−15115

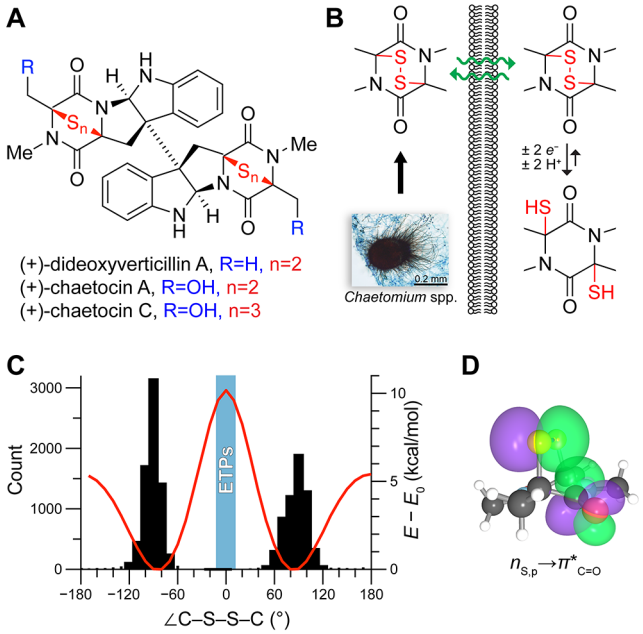

Figure 1. Properties of ETPs. (A) Chemical structures of representative ETPs. (B) Depiction of the biological origin and cellular entry of an ETP. (C) Graph of the distribution of cystinyl C^{β}–S^{γ}–$S^{\gamma\prime}$–$C^{\beta\prime}$ dihedral angles in high-resolution (<3.0 Å) protein crystal structures (black; Table S1), dependence of the energy of the disulfide bond in dimethyl disulfide on the C–S–S–C dihedral angle (red; Table S2), and range of C–S–S–C dihedral angles in crystalline ETPs (blue; Table S3). (D) Overlap of the $n_{S,p}$ and $\pi_{C=O}$* orbitals (green) in a model ETP derived from *N*-methylalanine. Calculations were at the M06-2X/6-311+G(d,p) level of theory.

for this compensation would be apparent in the X-ray structures of the natural products. In the 1970s, pioneering crystallographic analyses of Bürgi and Dunitz revealed that the optimal angle for nucleophilic attack at a carbonyl group occurs at ∼107°.[13] Approach at other angles leads to less efficient orbital overlap, resulting in a smaller donation of

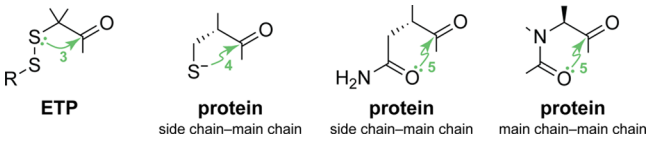

Figure 3. Depiction of known $n\rightarrow\pi^*$ interactions in biomolecules, which occur via rings of the indicated size. ETP, 3, this work; protein, 4;[16] protein, 5 (side chain–main chain);[17] protein, 5 (main chain–main chain).[11,15,18]

electron density. We find that values of the S···C=O angle in ETPs are indeed close to the Bürgi–Dunitz trajectory, having a range of 119–128° (Figure 2B).

Next, we used quantum chemistry to investigate the chemical forces that stabilize the strained disulfide bridge of ETPs. We found that the disulfide 3p lone pairs engage intimately with the amide carbonyl groups of the diketopiperazine scaffold. We then employed second-order perturbation theory calculations within the natural bond orbital theory formalism to investigate the strength of the interaction.[14] We found that $n\rightarrow\pi^*$ interactions between the sulfur 3p lone pair (n) and the carbonyl π antibonding orbital (π^*) have energies of 3–5 kcal/mol (Table S4). Compared to the $n\rightarrow\pi^*$ interactions studied previously in proteins (∼0.25 kcal/mol),[15] these $n\rightarrow\pi^*$ interactions are extraordinary.

The $n\rightarrow\pi^*$ interactions in ETPs are rarefied not only in their strength but also in their context. They occur within a 3-membered ring (Figure 3). Significant $n\rightarrow\pi^*$ interactions are known to occur within important 4- and 5-membered rings of proteins (Figure 3).[11,15−18] $n\rightarrow\pi^*$ interactions to carbonyl groups have also been observed within some larger rings.[19,20]

Anticipating that smaller disulfide bond lengths, r_{S-S}, would be consistent with reduced electron–electron repulsion between the 3p orbitals of the two sulfur atoms due to donation of electron density from each $n_{S,p}$ into the π^* orbital of a carbonyl group, we looked for evidence of $n\rightarrow\pi^*$ interactions in the structure of natural ETPs. Specifically, we measured values of r_{S-S} in natural ETPs, calculated values of $\Sigma E_{n\rightarrow\pi^*}$, and found a correlation (Figure 2C). Likewise,

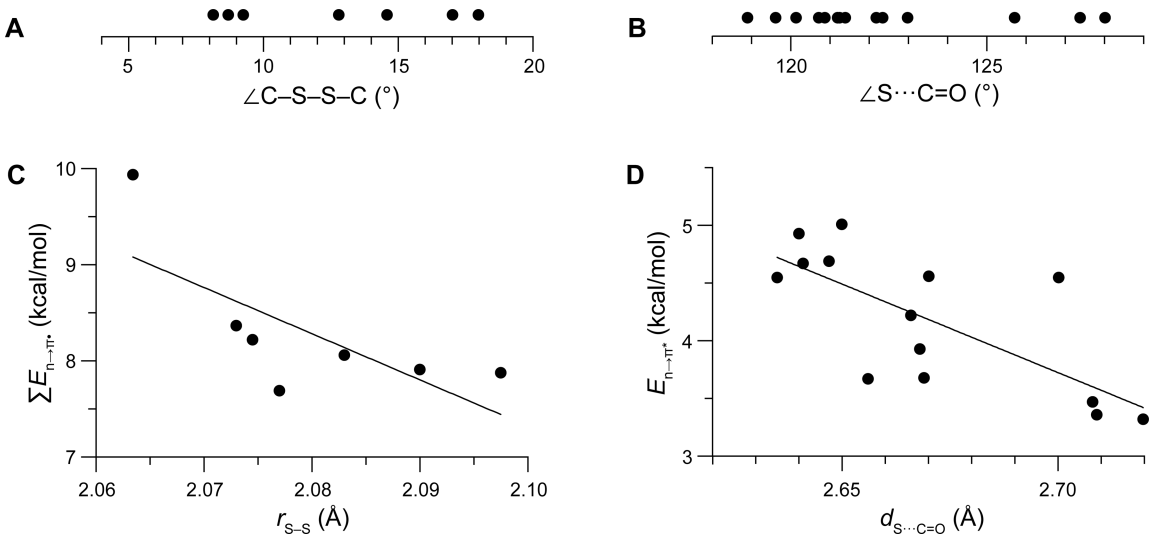

Figure 2. Graphs showing measured and calculated parameters of natural ETPs. (A) C–S–S–C dihedral angles. (B) Angle of the sulfur donor to the carbonyl acceptor. (C) Cumulative energy of $n\rightarrow\pi^*$ interactions versus sulfur–sulfur bond length (R^2 = 0.52). (D) Energy of an $n\rightarrow\pi^*$ interaction versus its sulfur to carbonyl-carbon distance (R^2 = 0.53). Energies on the ordinate were computed at the M06-2X/6-311+G(d,p) level of theory. Chemical structures and data are in Tables S3 and S4.

https://dx.doi.org/10.1021/jacs.0c06477
J. Am. Chem. Soc. 2020, 142, 15107−15115

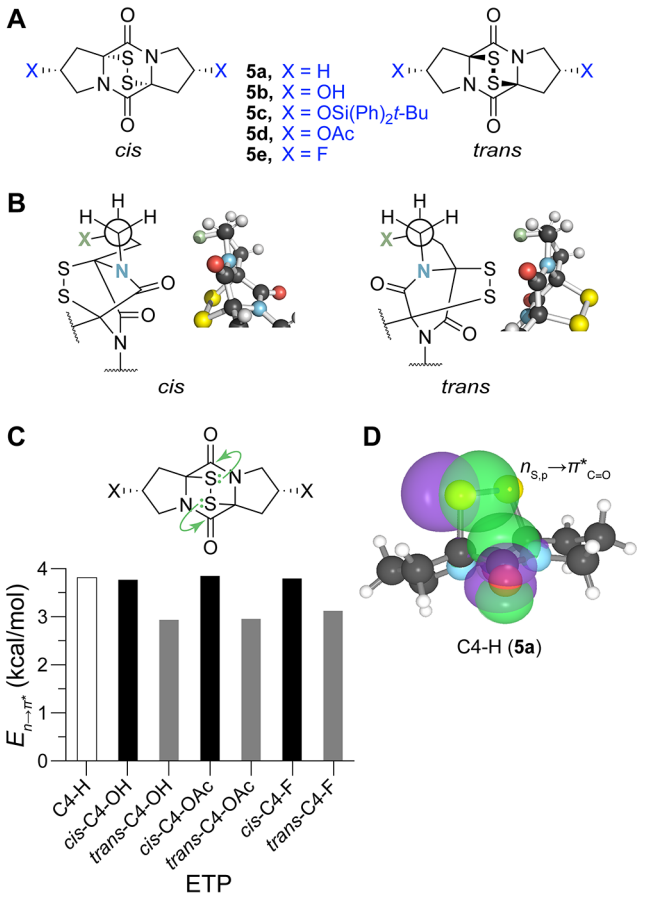

Figure 4. Design principles for ETP model systems. (A) C4-substituted series of symmetric bisprolyl-ETPs **5**. (B) Newman projection of ETPs illustrating the gauche effect in cis and trans configurations. (C) Symmetrical $n\rightarrow\pi^*$ interactions in model ETPs and their calculated energies. (D) Overlap of $n_{S,p}$ and $\pi_{C=O}^*$ orbitals in bisprolyl-ETP **5a**. Calculations were at the M06-2X/6-311+G(d,p) level of theory.

Scheme 1. Retrosynthesis of Designed Bisprolyl-ETPs (5)

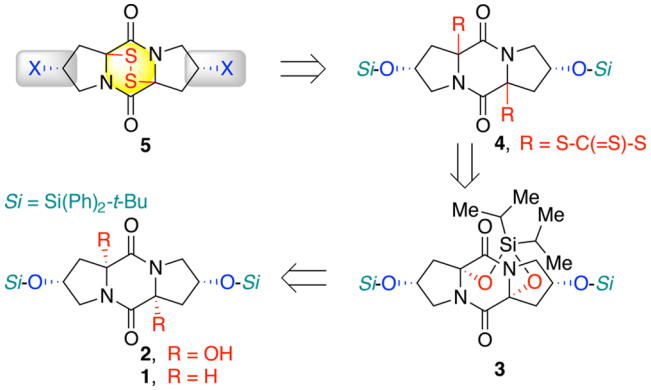

measured values of the donor–acceptor distance, $d_{S\cdots C=O}$, decrease as values of $E_{n\rightarrow\pi^*}$ increase (Figure 2D). Although neither of these correlations is strong, they are consistent with an $n\rightarrow\pi^*$ interaction.

Design of ETP Model Systems. To examine the physicochemical underpinnings of the ETP substructure in greater detail, we designed a symmetrical ETP model that reduces the complexity of the disulfide exchange equilibria

Scheme 2. Synthesis of Substituted ETPs (5c)[a]

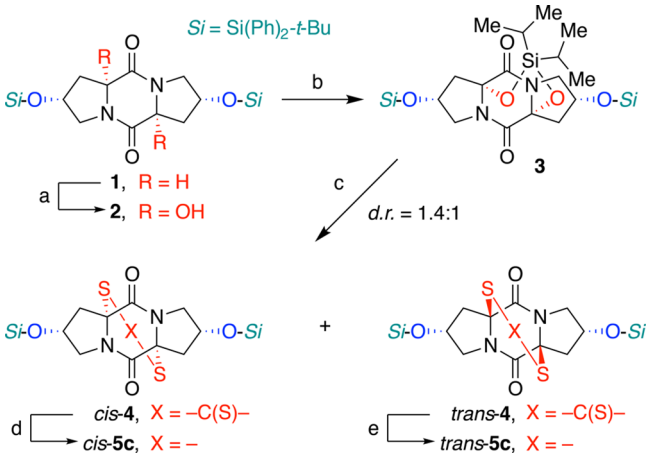

[a]Conditions: (a) Py_2AgMnO_4, pyridine, $PhCF_3$, 23 °C, 2 h 20 min, 40%. (b) *i*-Pr_2SiCl_2, NEt_3, DMAP, DMF, 0 → 23 °C, 95%. (c) Sodium *p*-methoxybenzyl trithiocarbonate, TFA, CH_2Cl_2, 23 °C, 1.75 h, 51% (*cis*-**4**) + 39% (*trans*-**4**). (d) Ethanolamine, acetone, 0 → 23 °C, 30 min; then KI_3, pyridine, CH_2Cl_2, 90%. (e) Ethanolamine, acetone, 0 → 23 °C, 45 min; then KI_3, pyridine, CH_2Cl_2, 71%. *Si* = $Si(Ph)_2$*t*-Bu.

Scheme 3. Synthesis of C4-Substituted ETPs 5b and 5d[a]

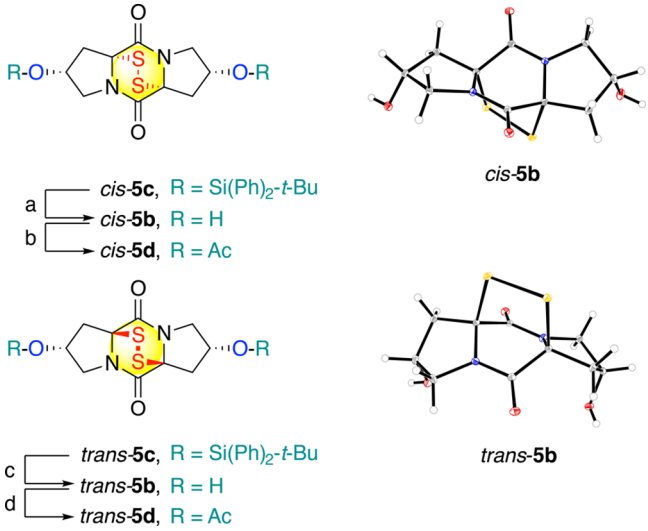

[a]Conditions: (a) HF-pyridine, pyridine, THF, 0 → 23 °C, 40 h, 81%. (b) AcCl, pyridine, CH_2Cl_2, 0 → 23 °C, 6 h, 78%. (c) HF-pyridine, pyridine, THF, 0 → 23 °C, 18 h, 82%. (d) AcCl, pyridine, CH_2Cl_2, 0 → 23 °C, 8 h, 92%. In the ORTEP representation of ETPs **5b**, the thermal ellipsoids are drawn at 50% probability.

while providing opportunities to examine the impact of substituents on the disulfide bond. We envisioned bisprolyl-ETP **5a** (Figure 4A) and the C4-substituted derivatives **5b–e** as an ideal platform for rigorous structural and physicochemical analyses.[21] Substitution of the pyrrolidine rings at C4 is known to influence ring puckering via a gauche effect (Figure 4B). Specifically, *R*-configured electron-withdrawing groups at the C-4 position in a proline residue favor C4-*exo* ring puckering, and *S*-configured groups favor C4-*endo* ring puckering.[22,23] Thus, we chose to introduce fluoro, hydroxy, and acetoxy groups in *R* or *S* configurations at C4 of bisprolyl-ETPs, giving rise to compounds in which the 4 substituent and

https://dx.doi.org/10.1021/jacs.0c06477
J. Am. Chem. Soc. 2020, 142, 15107–15115

Scheme 4. Synthesis of *cis*- and *trans*-C4-F ETPs 5e[a]

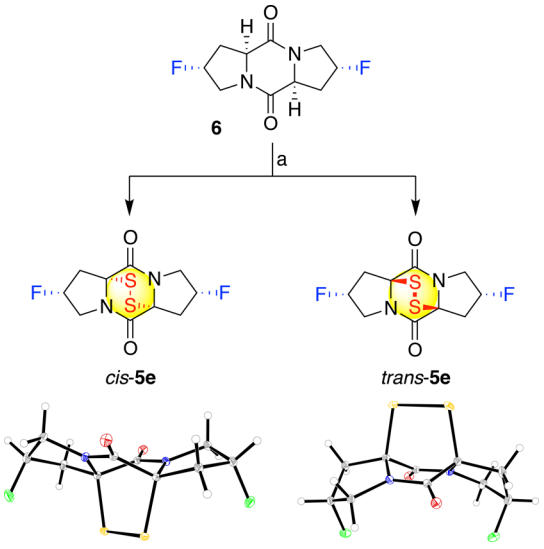

[a]Conditions: (a) NaHMDS, S_8, THF, 23 °C, 2 h; $NaBH_4$, THF, EtOH, 0 → 23 °C, 2 h; KI, I_2, pyridine, DCM, 23 °C, 5 min, 19% (*cis*-**5e**) + 5% (*trans*-**5e**). In the ORTEP representation of ETPs **5e**, the thermal ellipsoids are drawn at 50% probability.

Scheme 5. Stereochemical Assignment of Sulfides 7 and 8

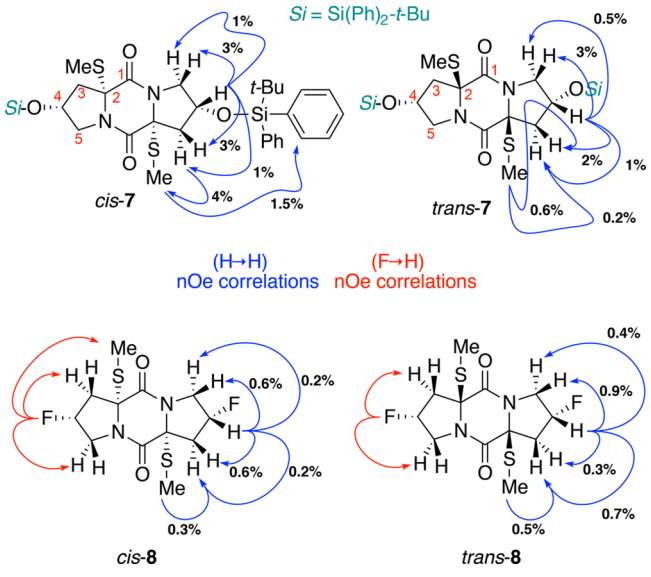

disulfide bond are on the same face of the fused rings (cis) or on opposite faces (trans). Our calculations revealed that, as intended, substitution at the C4 position induces conformational changes in ETP **5** that, in turn, modulate orbital overlap and thus the energy of the $n\rightarrow\pi^*$ interactions (Figures 4C and 4D). In particular, the cis and trans configurations differ by ∼1 kcal/mol.

Synthesis of C4-Substituted Bisprolyl-ETPs. As described above, we pursued the synthesis of the *cis*- and *trans*-C4-substituted bisprolyl-ETPs **5** (Figure 4A) to evaluate the structural parameters that modulate the reduction potential of the disulfide bond. The unsubstituted bisprolyl-ETP **5a** (Figure 2, C4−H) had been used previously as a reference in cytotoxicity studies.[21,24]

The general approach we used to access bisprolyl-ETPs **5** is outlined in Scheme 1. We envisioned that dithiepanethione **4** could serve as an effective precursor to ETP **5** as we have demonstrated en route to related systems.[4,7] We anticipated that the late-stage introduction of the trithiocarbonate to the bisprolyl framework could provide access to both *cis*- and *trans*-dithiepanethiones **4** from a common precursor dioxasilane **3** (Scheme 1). The silyl bridge of dioxasilane **3** derived from silylation of DKP-diol **2** was anticipated to offer superior solubility in organic solvents, facilitating the sulfidation step. We expected that DKP-diol **2** could be prepared using our permanganate-mediated dihydroxylation[25] of DKP **1**, which itself is a cyclodipeptide derivative of the commercially available and inexpensive *trans*-4-hydroxy-L-proline. As described below, we found this synthetic approach to be advantageous in accessing C4-substituted derivatives through late-stage diversification.

As illustrated in Scheme 2, we targeted *cis*- and *trans*-C4-silyloxy ETPs **5c** as common intermediates en route to other C4-substituted epidisulfides **5** (Figure 4A). Our synthesis commenced with the known silylation of *trans*-C4-hydroxy-L-proline followed by aryl boronic acid-catalyzed dehydrative−dimerization to corresponding DKP **1**.[26] The permanganate-mediated hydroxylation[4,25] of DKP **1** using bis(pyridine)-silver(I) permanganate[27] in a pyridine−α,α,α-trifluorotoluene mixture (1:1) afforded DKP-diol **2** in 40% yield.[28] We found that exposure of diol **2** to monosodium *p*-methoxybenzyl trithiocarbonate, a reagent for *cis*-sulfidation of DKP-diols,[8b] and trifluoroacetic acid in dichloromethane led to formation of *cis*- and *trans*-dithiepanethiones **4** (dr 2.2:1) in 61% and 19% yield, respectively. Nonetheless, as shown in Scheme 2, we found it advantageous to utilize dioxasilane **3** as the substrate for the sulfidation reaction since it afforded the *cis*- and *trans*-dithiepanethiones **4** (dr 1.4:1) in 51% and 39% yield, respectively. These dithiepanethiones were readily separated and efficiently converted to the corresponding *cis*- and *trans*-C4-silyloxy epidisulfides **5c** in 90% and 71% yield, respectively, upon aminolysis followed by oxidative disulfide formation with potassium triiodide.[4,29]

Having secured access to epidisulfides **5c**, it was necessary to determine their relative and absolute stereochemistry prior to advancing toward the water-soluble derivatives for our study (vida infra). As shown in Scheme 3, *cis*- and *trans*-C4-silyloxy ETPs **5c** were desilylated upon exposure to hydrogen fluoride in a pyridine−THF mixture (1:9) to give *cis*- and *trans*-C4-OH ETPs **5b** in 81% and 82% yield, respectively. We were able to obtain crystals of *cis*- and *trans*-C4-OH ETPs **5b** suitable for X-ray diffraction by slow evaporation from dichloromethane−methanol (10:1). We found structural information such as the S−S bond length and S···C═O angle of approach observable in the solid state corelated to both the strength of $n\rightarrow\pi^*$ interactions as well as the reduction potential of C4-substituted bisprolyl-ETPs (vida infra). Subsequent treatment of *cis*- and *trans*-C4-OH ETPs **5b** with acetyl chloride and pyridine in dichloromethane led to isolation of *cis*- and *trans*-C4-OAc ETPs **5d** in 78% and 92% yield, respectively. We were intrigued by the possibility of late-stage introduction of the fluoro substituents to access *cis*- and *trans*-C4-F ETPs **5e** by deoxofluorination of the available ETPs **5b**−**d**.[30] Yet, despite a wealth of precedent for stereoinvertive deoxofluorination on C4-OH-substituted proline derivatives,[31] there are no reported examples of deoxofluorination in the presence of a disulfide.[32] We found that exposure of *cis*-C4-silyloxy ETP **5c** to triethylamine trihydrofluoride (10 equiv) and triethylamine (5 equiv) in dichloromethane at 23 °C for 21 h afforded *cis*-

https://dx.doi.org/10.1021/jacs.0c06477
J. Am. Chem. Soc. 2020, 142, 15107−15115

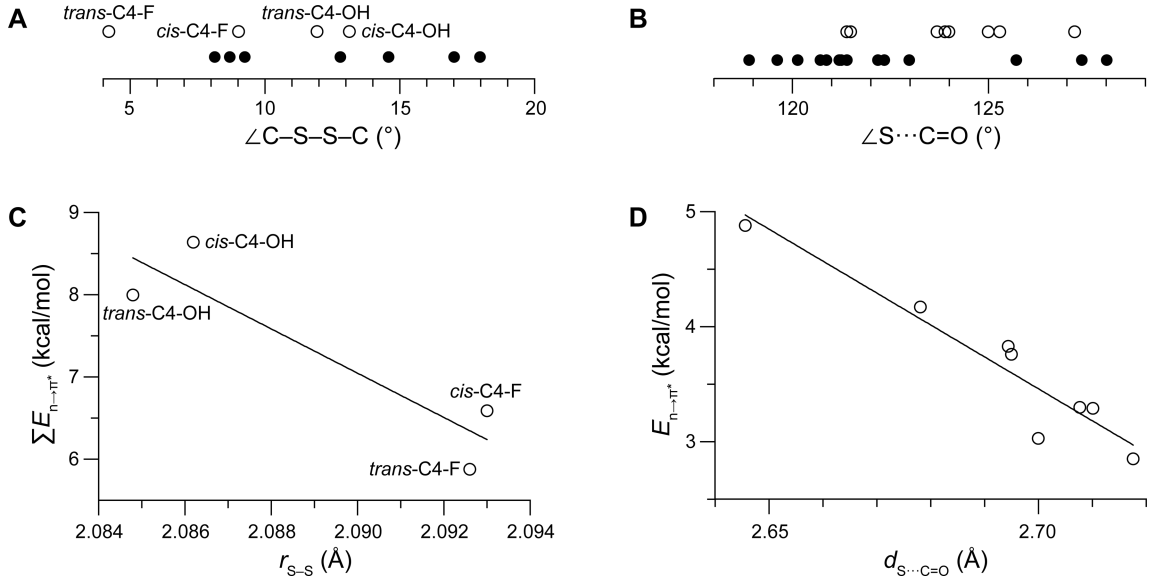

Figure 5. Graphs showing measured and calculated parameters of synthetic ETPs with known crystal structures. (A) C−S−S−C dihedral angles (○). (B) Angle of the sulfur donor to the carbonyl acceptor (○). (C) Cumulative energy of $n\rightarrow\pi^*$ interactions versus sulfur−sulfur bond length (R^2 = 0.82). (D) Energy of an $n\rightarrow\pi^*$ interaction versus its sulfur to carbonyl-carbon distance (R^2 = 0.90). In A and B, data for natural ETPs (●) are shown again for comparison. Energies on the ordinate were computed at the M06-2X/6-311+G(d,p) level of theory. Data are listed in Table S5.

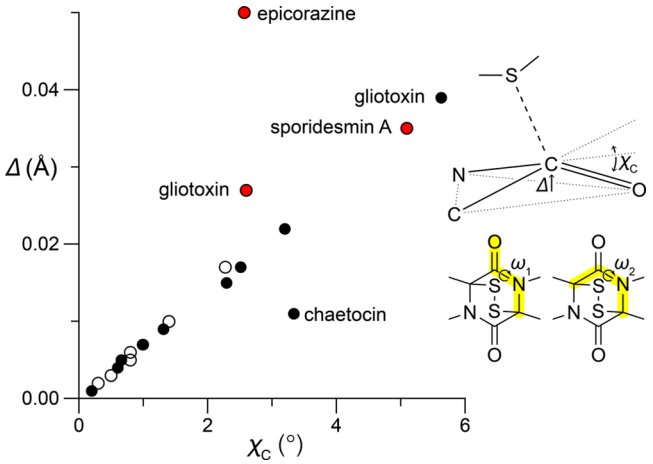

Figure 6. Graph showing two measures of the pyramidalization of carbonyl-group acceptors toward sulfur donors in natural (●) and synthetic (○) ETPs in known crystal structures. Values of Δ were determined with the CCDC program Mercury. Values of χ_C were determined from the ω_1 and ω_2 dihedral angles with the equation $\chi_C = \omega_1 - \omega_2 + \pi(\mathrm{mod}\ 2\pi)$.[39] Origin of outlying points is indicated: (red) carbonyl groups that accept hydrogen bonds in the crystal structure.

Table 1. Reduction Potentials ($E^{\circ\prime}$) of Synthetic ETPs

ETP	$E^{\circ\prime}$ (mV)[a]	$E^{\circ\prime}_{-n\rightarrow\pi^*}$ (mV)[a]
C4−H (**5a**)	−254 ± 5	
cis-C4-OH (*cis*-**5b**)	−244 ± 7	−57 ± 7
trans-C4-OH (*trans*-**5b**)	−242 ± 6	−69 ± 6
cis-C4-OAc (*cis*-**5d**)	−230 ± 4	
trans-C4-OAc (*trans*-**5d**)	−267 ± 3	
cis-C4-F (*cis*-**5e**)	−264 ± 3	−121 ± 3
trans-C4-F (*trans*-**5e**)	−221 ± 5	−93 ± 5

[a]Values (±SD) of $E^{\circ\prime}$ were derived from the thiol and disulfide concentrations of a solution equilibrated with reduced and oxidized lipoic acid.[37] [b]Values of $E^{\circ\prime}_{-n\rightarrow\pi^*}$ were calculated at 25 °C from the measured values of $E^{\circ\prime}$ and the calculated values of $\Sigma E_{n\rightarrow\pi^*}$ for synthetic ETPs with known crystal structures (Figure 5C)

C4-OH ETP **5b** and that exposure of the reaction mixture to morpholinodifluorosulfinium tetrafluoroborate (XtalFluor-M, 4 equiv) at −78 °C, followed by warming, provided ent-*trans*-C4-F ETP **5e** in 4% yield. Similarly, exposure of *trans*-C4-silyloxy ETP **5c** to identical conditions gave ent-*cis*-C4-F ETP **5e** in 7% yield. Alternatively, we sought to pursue a complementary approach to C4−F-ETPs **5e** via use of the corresponding C4−F DKP **6** (Scheme 4).[33] Condensation of *N*-Boc-*trans*-4-F-L-proline with *trans*-4-F-L-proline-OMe hydrochloride[33] followed by trifluoroacetic acid-promoted cyclization of the resulting dipeptide gave the desired DKP **6** in 87% yield.[29] Permanganate-mediated dihydroxylation of DKP **6** was not optimal due to incomplete dihydroxylation and complications arising from the water solubility of the resulting DKP-diol.

Reasoning that the observed challenges were in part due to the inductive influence of the C4−F substituent,[4,25a] we examined the use of base-promoted electrophilic sulfidation. Exposure of DKP **6** to a solution of elemental sulfur and sodium hexamethyldisilazide (NaHMDS) in tetrahydrofuran[21,34] followed by sequential reduction with sodium borohydride and oxidation with potassium triiodide gave separable mixtures of *cis*-C4-F and *trans*-C4-F epipolysulfides. The polysulfide mixtures were subjected separately to another round of reduction and oxidation to give *cis*- and *trans*-C4−F epidisulfides **5e**, offering an alternative approach to access ETPs **5e** for our planned study. Importantly, we obtained crystals suitable for X-ray diffraction of *cis*-C4−F epidisulfide **5e** by recrystallization from acetone−hexanes (3:1) and of *trans*-C4−F epidisulfide **5e** by slow evaporation of a saturated solution in acetone−hexanes (1:7), providing further opportunities for detailed structural analysis (Scheme 4). Because complete stereochemical assignment of *cis*- and *trans*-ETPs **5b−e** is critical to our analysis of the structural features impacting the reduction potential of the epidisulfide bridge,

https://dx.doi.org/10.1021/jacs.0c06477
J. Am. Chem. Soc. 2020, 142, 15107−15115

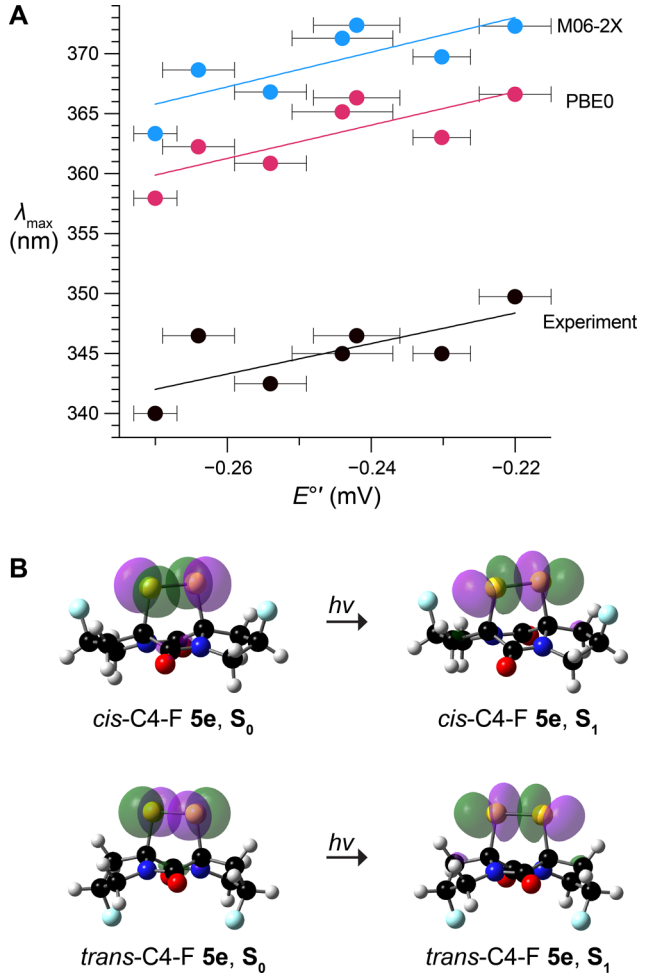

Figure 7. Correlations between the UV−vis absorption and the reduction potential of the disulfide bond in synthetic ETPs. (A) Graph showing the wavelength of maximal absorption versus reduction potential. Values of λ_{max} were measured experimentally (black; $R^2 = 0.53$) or calculated with the M06-2X (blue; $R^2 = 0.62$) or PBE0 (red; $R^2 = 0.62$) DFT functionals. Data are listed in Table S6. (B) Natural transition orbitals for the $S_0 \rightarrow S_1$ transition of *cis*-C4-F ETP **5e** (top) and *trans*-C4-F ETP **5e** (bottom).

prior to obtaining the X-ray structure for ETPs **5b** and **5e**, we conducted detailed nuclear magnetic resonance (NMR) studies of related derivatives (Scheme 5). We anticipated differentiating the diastereomeric pairs of *cis*- and *trans*-epidisulfides **5b** and **5e** by reductive methylation and selective nuclear Overhauser effect (NOE) NMR experiments relative to the C4-α-stereochemistry encoded within *trans*-4-hydroxy-L-proline.[8a,35] Accordingly, the reductive methylation of ETPs **5c** and **5e** using sodium borohydride and methyl iodide afforded bis(methylthioether) DKPs **7** and **8**, respectively.[29] The stereochemistry of the C2 methyl sulfide was secured via NOE correlations from the *S*-methyl to the C4-stereocenter through the $C3H_{\alpha/\beta}$ and $C5H_{\alpha/\beta}$ protons as illustrated in Scheme 5. Thestereochemical assignments of *cis*- and *trans*-sulfides **7** and **8** were consistent with the X-ray crystal structures of the corresponding *cis*- and *trans*-ETPs **5b** and **5e**, respectively.

C4-Substitution Modulates $n\rightarrow\pi^*$ Interaction in Model ETPs. With the model compounds in hand, we were poised to deconvolute relationships between the structural and the physicochemical properties of ETPs. Consistent with our hypothesis about the role of $n\rightarrow\pi^*$ interactions in ETPs, we found that trends in the synthetic bisprolyl-ETPs mirror those of natural ETPs (cf. Figures 2 and 5). The most striking trend is depicted in Figure 5D, where a change in the S···C=O distance with a range of 0.07 Å corresponded with a change in the $E_{n\rightarrow\pi^*}$ interaction of 2 kcal/mol.

Crystallographic Signature of $n\rightarrow\pi^*$ Interactions. Following the precedent of Bürgi and Dunitz,[13] the most compelling experimental signature of an $n\rightarrow\pi^*$ interaction has become the pyramidalization of the acceptor carbonyl group toward the electron-pair donor.[36] That signature is evident in the crystal structures of both ETP natural products and model ETPs **5b** and **5e** (Figure 6). Moreover, the interaction is coupled with hydrogen bonding in the crystal structures of gliotoxin, sporidesmin A, and epicorazine, which can lead to aberrant pyramidalization.

Disulfide Photophysics Enables Electrochemical Measurements. The C−S−S−C dihedral angle (θ) correlates with the wavelength of its maximal absorption.[12] For example, oxidized lipoic acid ($E^{\circ\prime} = -288$ mV[38]) has C−S−S−C dihedral angle near $\theta = 45°$ and an absorption maximum of 330 nm (Figure S1),[12] which is distinct from those of ETPs (Table S6), though there is some spectral overlap (Figures S2 and S3). Using this assay, we were able to detect the concentration of lipoic acid in an ETP ⇄ lipoic acid equilibrium to a concentration as low as 1 μM.

We found that the reduction potentials of synthetic ETPs range from −221 to −267 mV (Table 1). Thus, each synthetic ETP would be reduced nearly completely upon cytosolic entry. The stability afforded by two $n\rightarrow\pi^*$ interactions decreases the ETP $E^{\circ\prime}$ values substantially (Table 1), enabling the disulfide bond to remain intact in a wide range of physiological environments, including the endoplasmic reticulum (which has $E^{\circ\prime} \approx -210$ mV[40]). In the cytosol, however, the high ratio of reduced glutathione to oxidized glutathione leads to a reduction potential of $E^{\circ\prime} \approx -320$ mV.[40b,41] Hence, the measured reduction potentials indicate that the $n\rightarrow\pi^*$ interactions in ETPs are responsible for a balance between extracellular stability and intracellular activity. Without its $n\rightarrow\pi^*$ interactions, the disulfide bond in an ETP would be much less stable than, for example, that in dithietane ($C_2H_4S_2$; $E^{\circ\prime} = -239$ mV[38]), which has a disulfide bond within a 4-membered ring. Conversely, if the $n\rightarrow\pi^*$ interactions were too strong, intracellular reduction to the active bisthiol form would not occur.

The $n\rightarrow\pi^*$ interactions within ETPs make their reduction potential responsive to the environment. Specifically, $n\rightarrow\pi^*$ interactions to a carbonyl group are stronger in protic environments because a hydrogen bond polarizes the carbonyl group, making it a superior acceptor of an $n\rightarrow\pi^*$ interaction.[42] Thus, we anticipate that the disulfide bond in an ETP will be more vulnerable to reduction in a hydrophobic or otherwise desolvated environment, such as the ligand-binding site of a protein or the active site of an enzyme.

Energetic Basis for ETP Electrochemical Equilibria. Finally, we sought to understand the reduction potentials of ETPs in light of the strain in their disulfide bonds. We found a correlation between two energies: the reduction potential of the disulfide bond and the wavelength of its maximal absorption (Figure 7). Specifically, the reduction potential of an ETP is larger (which is indicative of being more easily reduced to the bisthiol) when the wavelength of maximal absorption is larger (which correlates with a more eclipsed C−

https://dx.doi.org/10.1021/jacs.0c06477
J. Am. Chem. Soc. 2020, 142, 15107−15115

S−S−C dihedral angle[12]). To our knowledge, this is the first example of a correlation between these two manifestations of energy: $E^{\circ\prime} \propto \lambda_{max}$. This correlation is consistent with the intrinsic stability (Figure 1C) and photophysics[12] of disulfide bonds.

To investigate the electronic basis of the relationship between $E^{\circ\prime}$ and λ_{max}, we computed the natural transition orbitals (NTOs) of synthetic model ETPs **5**. At such eclipsed C−S−S−C dihedral angles, the ground state ($\mathbf{S_0}$) is composed primarily of p-type lone pair density (Figure 7B).[12] Promotion of electrons to the first excited state ($\mathbf{S_1}$) populates an NTO with antibonding character, consistent with the observed correlation of $E^{\circ\prime}$ and λ_{max} (Figure 7A).

CONCLUSIONS

We discovered an important aspect of ETP natural products: strong $n\rightarrow\pi^*$ interactions in which electron density is donated from the sulfur atoms of the disulfide bond into the carbonyl groups of the diketopiperazine. Two strong $n\rightarrow\pi^*$ interactions in each ETP nearly completely compensate for the ∼10 kcal/mol of instability imposed by the eclipsed conformation of the disulfide bond. This discovery could elucidate structure−activity relationships of ETPs and inform the design of new ETPs with desirable properties. Moreover, the utility of $n\rightarrow\pi^*$ interactions in stabilizing disulfide bonds could be applicable in other molecular contexts.

ASSOCIATED CONTENT

Supporting Information

The Supporting Information is available free of charge at https://pubs.acs.org/doi/10.1021/jacs.0c06477.

ETP *cis*-**5b** CCDC 1965015 (CIF)
ETP *trans*-**5b** CCDC 1965016 (CIF)
ETP *cis*-**5e** CCDC 1965017 (CIF)
ETP *trans*-**5e** CCDC 1965018 (CIF)
PDB-derived ∠C−S−S−C values; calculated $E - E_0$ values; epidithiodiketopiperazine natural product structures; data used to compose plots in Figure 2; data used to compose plots in Figure 5; data used to compose plots in Figure 7; UV−vis spectroscopy of oxidized lipoic acid; UV−vis absorption spectra and first-derivative spectra of synthetic ETPs; UV−vis absorption first-derivative spectral data of synthetic ETPs; experimental and computational procedures, crystallographic data; computational data; ^{1}H, ^{13}C, and ^{19}F NMR spectra (PDF)

AUTHOR INFORMATION

Corresponding Authors

Mohammad Movassaghi − *Department of Chemistry, Massachusetts Institute of Technology, Cambridge, Massachusetts 02139, United States;* orcid.org/0000-0003-3080-1063; Email: movassag@mit.edu

Ronald T. Raines − *Department of Chemistry, Massachusetts Institute of Technology, Cambridge, Massachusetts 02139, United States;* orcid.org/0000-0001-7164-1719; Email: rtraines@mit.edu

Authors

Henry R. Kilgore − *Department of Chemistry, Massachusetts Institute of Technology, Cambridge, Massachusetts 02139, United States;* orcid.org/0000-0003-4851-9656

Chase R. Olsson − *Department of Chemistry, Massachusetts Institute of Technology, Cambridge, Massachusetts 02139, United States;* orcid.org/0000-0001-9021-3664

Kyan A. D'Angelo − *Department of Chemistry, Massachusetts Institute of Technology, Cambridge, Massachusetts 02139, United States;* orcid.org/0000-0002-9688-5143

Complete contact information is available at: https://pubs.acs.org/10.1021/jacs.0c06477

Author Contributions

†H.R.K. and C.R.O. contributed equally.

Funding

K.A.D. acknowledges the Natural Sciences and Engineering Research Council of Canada (NSERC) for a PGS-D3 scholarship. This work was supported by Grants R01 GM089732 and R01 GM044783 (NIH) and made use of the Extreme Science and Engineering Discovery Environment (XSEDE), which is supported by Grant ACI-1548562 (NSF).

Notes

The authors declare no competing financial interest.

ACKNOWLEDGMENTS

We thank Dr. Charlene Tsay and Dr. Peter Müller (Department of Chemistry, Massachusetts Institute of Technology) for assistance with single-crystal X-ray diffraction. M.M. and C.R.O. thank Dr. Brandon M. Nelson for helpful discussions related to DKP-dioxasilanes.

REFERENCES

(1) (a) Darwin, C. *On the Origin of Species by Means of Natural Selection, or Preservation of Favoured Races in the Struggle for Life*; John Murray: London, UK, 1859. (b) Mayr, E. *The Growth of Biological Thought: Diversity, Evolution, and Inheritance*; Harvard University Press: Cambridge, MA, 1982.

(2) (a) Keller, N. P. Fungal secondary metabolism: Regulation, function and drug discovery. *Nat. Rev. Microbiol.* **2019**, *17*, 167−180. (b) Künzler, M. How fungi defend themselves against microbial competitors and animal predators. *PLoS Pathog.* **2018**, *14*, No. e1007184.

(3) (a) Hino, T.; Nakagawa, M. Chemistry and reactions of cyclic tautomers of tryptamines and tryptophans. In *The Alkaloids: Chemistry and Pharmacology*, Brossi, A., Ed.; Academic Press: New York, 1989; Vol. *34*, pp 1−75. (b) Waring, P.; Beaver, J. Gliotoxin and related epipolythiodioxopiperazines. *Gen. Pharmacol.* **1996**, *27*, 1311−1316. (c) Gardiner, D. M.; Waring, P.; Howlett, B. J. The epipolythiodioxopiperazine (ETP) class of fungal toxins: Distribution, mode of action, functions, and biosynthesis. *Microbiology* **2005**, *151*, 1021−1032. (d) Kim, J.; Movassaghi, M. Biogenetically inspired syntheses of alkaloid natural products. *Chem. Soc. Rev.* **2009**, *38*, 3035−3050. (e) Jiang, C.-S.; Guo, Y.-W. Epipolythiodioxopiperazines from fungi: Chemistry and bioactivities. *Mini-Rev. Med. Chem.* **2011**, *11*, 728−745. (f) Welch, T. R.; Williams, R. M. Epidithiodioxopiperazines: Occurence, synthesis, and biogenesis. *Nat. Prod. Rep.* **2014**, *31*, 1376−1404.

(4) Kim, J.; Movassaghi, M. Biogenetically-inspired total synthesis of epidithioketopiperazines and related alkaloids. *Acc. Chem. Res.* **2015**, *48*, 1159−1171.

(5) (a) Vigushin, D. M.; Mirsaidi, N.; Brooke, G.; Sun, C.; Pace, P.; Inman, L.; Moody, C. J.; Coombes, R. C. Gliotoxin is a dual Inhibitor of farnesyltransferase and geranylgeranyltransferase I with antitumor activity against breast cancer *in vivo*. *Med. Oncol.* **2004**, *21*, 21−30. (b) Zheng, C. J.; Kim, C. J.; Bae, K. S.; Kim, Y.; Kim, W. G. Bionectins A−C, epidithiodioxopiperazines with anti-MRSA activity from *Bionectra byssicola* F120. *J. Nat. Prod.* **2006**, *69*, 1816−1819. (c) Isham, C. R.; Tibodeau, J. D.; Jin, W.; Xu, R.; Timm, M.; Bible, K.

C. Chaetocin: A promising new antimyeloma agent with *in vitro* and *in vivo* activity mediated via imposition of oxidative stress. *Blood* **2007**, *109*, 2579−2588. (d) Cook, K. M.; Hilton, S. T.; Mecinovic, J.; Motherwell, W.; Figg, W. D.; Schofield, C. J. Epidithiodiketopiperazines block the interaction between hypoxia-inducible-factor-1α (HIF-1α) and p300 by a zinc ejection mechanism. *J. Biol. Chem.* **2009**, *284*, 26831−26838. (e) Liu, F.; Liu, Q.; Yang, D.; Bollag, W. B.; Robertson, K.; Wu, P.; Liu, L. Verticillin A overcomes apoptosis resistance in human colon carcinoma through DNA methylation-dependent upregulation of BNIP3. *Cancer Res.* **2011**, *71*, 6807−6816. (f) Dubey, R.; Levin, M. D.; Szabo, L. Z.; Laszlo, C. F.; Kushal, S.; Singh, J. B.; Oh, P.; Schnitzer, J. E.; Olenyuk, B. Z. Suppression of tumor growth by designed dimeric epidithiodiketopiperazine targeting hypoxia-inducible transcription factor complex. *J. Am. Chem. Soc.* **2013**, *135*, 4537−4549. (g) Saleh, A. A.; Jones, G. W.; Tinley, F. C.; Delaney, S. F.; Alabbadi, S. H.; Fenlon, K.; Doyle, S.; Owens, R. A. Systems impact of zinc chelation by the epipolythiodioxopiperazine dithiol gliotoxin in *Aspergillus fumigatus*: A new direction in natural product functionality. *Metallomics* **2018**, *10*, 854−866. (h) Dewangan, J.; Srivastava, S.; Mishra, S.; Pandey, P. K.; Divakar, A.; Rath, S. K. Chetomin induces apoptosis in human triple-negative breast cancer cells by promoting calcium overload and mitochondrial dysfunction. *Biochem. Biophys. Res. Commun.* **2018**, *495*, 1915−1921. (i) Asquith, C. R.M.; Sil, B. C.; Laitinen, T.; Tizzard, G. J.; Coles, S. J.; Poso, A.; Hofmann-Lehmann, R.; Hilton, S. T. Novel epidithiodiketopiperazines as anti-viral zinc ejectors of the feline immunodeficiency virus (FIV) nucleocapsinprotein as a model for HIV infection. *Bioorg. Med. Chem.* **2019**, *27*, 4174−4184.

(6) For representative syntheses of ETPs, see: (a) Fukuyama, T.; Nakatsuka, S.-I.; Kishi, Y. Total synthesis of gliotoxin, dehydrogliotoxin, and hyalodendrin. *Tetrahedron* **1981**, *37*, 2045−2078. (b) Overman, L. E.; Sato, T. Construction of epdidithiodioxopiperazines by directed oxidation of hydroxyproline derived dioxopiperazines. *Org. Lett.* **2007**, *9*, 5267−5270. (c) Iwasa, E.; Hamashima, Y.; Fujishiro, S.; Higuchi, E.; Ito, A.; Yoshida, M.; Sodeoka, M. Total synthesis of (+)-chaetocin and its analogues: Their histone methyltransferase G9a inhibitory activity. *J. Am. Chem. Soc.* **2010**, *132*, 4078−4079. (d) Codelli, J. A.; Puchlopek, A. L. A.; Reisman, S. E. Enantioselective total synthesis of (−)-acetylaranotin, a dihydrooxepine epidithiodiketopiperazine. *J. Am. Chem. Soc.* **2012**, *134*, 1930−1933. (e) Takeuchi, R.; Shimokawa, J.; Fukuyama, T. Development of a route to chiral epidithiodioxopiperazine moieties and application to the asymmetric synthesis of (+)-hyalodendrin. *Chem. Sci.* **2014**, *5*, 2003−2006. (f) Baumann, M.; Dieskau, A. P.; Loertscher, B. M.; Walton, M. C.; Nam, S.; Xie, J.; Horne, D.; Overman, L. E. Tricyclic analogues of epidithiodioxopiperazine alkaloids with promising *in vitro* and *in vivo* antitumor activity. *Chem. Sci.* **2015**, *6*, 4451−4457.

(7) For representative syntheses of ETPs from our laboratory, see: (a) Kim, J.; Ashenhurst, J. A.; Movassaghi, M. Total synthesis of (+)-11,11′-dideoxyverticillin A. *Science* **2009**, *324*, 238−241. (b) Kim, J.; Movassaghi, M. General approach to epipolythiodiketopiperazine alkaloids: Total synthesis of (+)-chaetocins A and C and (+)-12,12′-dideoxychetracin A. *J. Am. Chem. Soc.* **2010**, *132*, 14376−14378. (c) Coste, A.; Kim, J.; Adams, T. C.; Movassaghi, M. Concise total synthesis of (+)-bionectins A and C. *Chem. Sci.* **2013**, *4*, 3191−3197.

(8) (a) Boyer, N.; Morrison, K. C.; Kim, J.; Hergenrother, P. J.; Movassaghi, M. Synthesis and anticancer activity of epipolythiodiketopiperazine alkaloids. *Chem. Sci.* **2013**, *4*, 1646−1657. (b) Olsson, C. R.; Payette, J. N.; Cheah, J. H.; Movassaghi, M. Synthesis of potent cytotoxic epidithiodiketopiperazines designed for derivatization. *J. Org. Chem.* **2020**, *85*, 4648−4662.

(9) (a) Borthwick, A. D. 2,5-Diketopiperazines: Synthesis, reactions, medicinal chemistry, and bioactive natural products. *Chem. Rev.* **2012**, *112*, 3641−3716. (b) Zong, L.; Bartolami, E.; Abegg, D.; Adibekian, A.; Sakai, N.; Matile, S. Epidithiodiketopiperazines: Strain-promoted thiol-mediated cellular uptake at the highest tension. *ACS Cent. Sci.* **2017**, *3*, 449−453. (c) Chuard, N.; Poblador-Bahamonde, A. I.; Zong, L.; Bartolami, E.; Hildebrandt, J.; Weigand, W.; Sakai, N.; Matile, S. Diselenolane-mediated cellular uptake. *Chem. Sci.* **2018**, *9*, 1860−1866.

(10) This strain is largely electronic rather than steric, as the analogous value of $E - E_0$ for H−S−S−H is ∼8 kcal/mol.

(11) Newberry, R. W.; Raines, R. T. The $n\rightarrow\pi^*$ interaction. *Acc. Chem. Res.* **2017**, *50*, 1838−1846.

(12) Kilgore, H. R.; Raines, R. T. Disulfide chromophores arise from stereoelectronic effects. *J. Phys. Chem. B* **2020**, *124*, 3931−3935.

(13) (a) Bürgi, H. B.; Dunitz, J. D.; Shefter, E. Geometric reaction coordinates. II. Nucleophilic addition to a carbonyl group. *J. Am. Chem. Soc.* **1973**, *95*, 5065−5067. (b) Bürgi, H. B.; Dunitz, J. D.; Shefter, E. Chemical reaction paths. IV. Aspects of O···C=O interactions in crystals. *Acta Crystallogr., Sect. B: Struct. Crystallogr. Cryst. Chem.* **1974**, *30*, 1517−1527. (c) Bürgi, H. B.; Dunitz, J. D.; Lehn, J. M.; Wipff, G. Stereochemistry of reaction paths at carbonyl centres. *Tetrahedron* **1974**, *30*, 1563−1572.

(14) (a) Weinhold, F.; Landis, C. R. *Discovering Chemistry with Natural Bond Orbitals*; John Wiley & Sons: Hoboken, NJ, 2012. (b) Weinhold, F. Natural bond orbital analysis: A critical overview of relationships to alternative bonding perspectives. *J. Comput. Chem.* **2012**, *33*, 2363−2379. (c) Glendening, E. D.; Badenhoop, J. K.; Reed, A. E.; Carpenter, J. E.; Bohmann, J. A.; Morales, C. M.; Landis, C. R.; Weinhold, F. *NBO 6.0*; Theoretical Chemistry Institute, University of Wisconsin—Madison: Madison, WI, 2013.

(15) Newberry, R. W.; Raines, R. T. Secondary forces in protein folding. *ACS Chem. Biol.* **2019**, *14*, 1677−1686.

(16) (a) Chakrabarti, P.; Pal, D. An electrophile−nucleophile interaction in metalloprotein structures. *Protein Sci.* **1997**, *6*, 851−859. (b) Kilgore, H. R.; Raines, R. T. $n\rightarrow\pi^*$ Interactions modulate the properties of cysteine residues and disulfide bonds in proteins. *J. Am. Chem. Soc.* **2018**, *140*, 17606−17611.

(17) Bartlett, G. J.; Newberry, R. W.; VanVeller, B.; Raines, R. T.; Woolfson, D. N. Interplay of hydrogen bonds and $n\rightarrow\pi^*$ interactions in proteins. *J. Am. Chem. Soc.* **2013**, *135*, 18682−18688.

(18) (a) Bretscher, L. E.; Jenkins, C. L.; Taylor, K. M.; DeRider, M. L.; Raines, R. T. Conformational stability of collagen relies on a stereoelectronic effect. *J. Am. Chem. Soc.* **2001**, *123*, 777−778. (b) Bartlett, G. J.; Choudhary, A.; Raines, R. T.; Woolfson, D. N. $n\rightarrow\pi^*$ Interactions in proteins. *Nat. Chem. Biol.* **2010**, *6*, 615−620. (c) Rahim, A.; Saha, P.; Jha, K. K.; Sukumar, N.; Sarma, B. K. Reciprocal carbonyl−carbonyl interactions in small molecules and proteins. *Nat. Commun.* **2017**, *8*, 78.

(19) For recent examples, see: (a) Vik, E. C.; Li, P.; Pellechia, P. J.; Shimizu, K. D. Transition-state stabilization by $n\rightarrow\pi^*$ interactions measured using molecular rotors. *J. Am. Chem. Soc.* **2019**, *141*, 16579−16583. (b) Hoang, H. N.; Wu, C.; Hill, T. A.; Dantas de Araujo, A.; Bernhardt, P. V.; Liu, L.; Fairlie, D. P. A novel long-range n to π^* interaction secures the smallest known a α-helix in water. *Angew. Chem., Int. Ed.* **2019**, *58*, 18873−18877. For intermolecular examples with metal thiolates, see: (c) Lewiński, J.; Bury, W.; Justyniak, I. Significance of intermolecular S···C(π) interaction involving M−S and −C=O centers in crystal structures of metal thiolate complexes. *Eur. J. Inorg. Chem.* **2005**, *2005*, 4490−4492.

(20) For counterexamples in nonnatural scaffolds, see: (a) Choudhary, A.; Raines, R. T. Signature of $n\rightarrow\pi^*$ interactions in α-helices. *Protein Sci.* **2011**, *20*, 1077−1081. (b) Muchowska, K. B.; Pascoe, D. J.; Borsley, S.; Smolyar, I.; Mati, I. K.; Adam, C.; Nichol, G. S.; Ling, K. B.; Cockroft, S. L. Reconciling electrostatic and $n\rightarrow\pi^*$ orbital contributions in carbonyl interactions. *Angew. Chem., Int. Ed.* **2020**, *59*, DOI: 10.1002/anie.202005739.

(21) For a prior synthesis of bisprolyl-ETP **5a**, see: Öhler, E.; Poisel, H.; Tataruch, F.; Schmidt, U. Syntheseversuche in der Reihe der 3.6-Epidithio-2.5-dioxo-piperazin-Antibiotika Gliotoxin, Sporidesmin, Aranotin und Chaetocin, IV. Synthese des Epidithio-L-prolyl-L-prolinanhydrids. *Chem. Ber.* **1972**, *105*, 635−641.

(22) (a) Shoulders, M. D.; Satyshur, K. A.; Forest, K. T.; Raines, R. T. Stereoelectronic and steric effects in side chains preorganize a protein main chain. *Proc. Natl. Acad. Sci. U. S. A.* **2010**, *107*, 559−564. (b) Pandey, A. K.; Naduthambi, D.; Thomas, K. M.; Zondlo, N. J.

Proline editing: A general and practical approach to the synthesis of functionally and structurally diverse peptides. Analysis of steric versus stereoelectronic effects of 4-substituted prolines on conformation within peptides. *J. Am. Chem. Soc.* **2013**, *135*, 4333−4363.
(23) The pyrrolidine ring puckering of 4-substituted proline residues can be altered upon incorporation into a DKP (Wennemers, H.; Nold, M. C.; Conza, M. M.; Kulicke, K. J.; Neuburger, M. Flexible but with a defined turn—Influence of the template on the binding properties of two-armed receptors. *Chem. - Eur. J.* **2003**, *9*, 442−448). Our synthetic ETPs are, however, more rigid than analogous DKPs, and calculations, the magnitude of their coupling constants, and the absence of disorder in their X-ray structures point to the dominance of the anticipated conformation..
(24) Bernardo, P. H.; Brasch, N.; Chai, C. L. L.; Waring, P. Novel redox mechanism for the glutathione-dependent reversible uptake of a fungal toxin in cells. *J. Biol. Chem.* **2003**, *278*, 46549−46555.
(25) (a) Bischoff, A. J.; Nelson, B. M.; Niemeyer, Z. L.; Sigman, M. S.; Movassaghi, M. Quantitative modeling of bis(pyridine)silver(I) permanganate oxidation of hydantoin derivatives: Guidelines for predicting the site of oxidiation in complex substrates. *J. Am. Chem. Soc.* **2017**, *139*, 15539−15547. (b) Haines, B. E.; Nelson, B. M.; Grandner, J. M.; Kim, J.; Houk, K. N.; Movassaghi, M.; Musaev, D. G. Mechanism of permanganate promoted dihydroxylation of complex diketopiperazines: Critical roles of counter cation and ion-pairing. *J. Am. Chem. Soc.* **2018**, *140*, 13375−13386.
(26) (a) Ishihara, K.; Ohara, S.; Yamamoto, H. 3,4,5-Trifluorobenzeneboronic acid as an extremely active amidiation catalyst. *J. Org. Chem.* **1996**, *61*, 4196. (b) Delaney, J. P.; Brozinski, H. L.; Henderson, L. C. Synergistic effects with a C_2-symmetric organocatalyst: The potential formation of a chiral catalytic pocket. *Org. Biomol. Chem.* **2013**, *11*, 2951−2960.
(27) Firouzabadi, H.; Vessal, B.; Naderi, M. Bispyridinesilver permanganate $[Ag(C_5H_5N)_2]MnO_4$: An efficient oxidizing reagent for organic substrates. *Tetrahedron Lett.* **1982**, *23*, 1847−1850.
(28) This solvent combination offered optimal substrate solubility and oxidation, as DKP **1** is insoluble in α,α,α-trifluorotoluene alone as solvent. Oxidation of DKP **1** with bis(pyridine)silver(I) permanganate in dichloromethane gave diol **2** in 8% yield with 46% recovered starting material, whereas the same oxidation in pyridine gave diol **2** in 12% yield with 63% recovered starting material.
(29) See the Supporting Information for further details.
(30) L'Heureux, A.; Beaulieu, F.; Bennett, C.; Bill, D. R.; Clayton, S.; LaFlamme, F.; Mirmehrabi, M.; Tadayon, S.; Tovell, D.; Couturier, M. Aminodifluorosulfinium salts: Selective fluorination reagents with enhanced thermal stability and ease of handling. *J. Org. Chem.* **2010**, *75*, 3401−3411.
(31) Newberry, R. W.; Raines, R. T. 4-Fluoroprolines: Conformational analysis and effects on the stability and folding of peptides and proteins. *Top. Heterocycl. Chem.* **2016**, *48*, 1−25.
(32) Thiocarbonyl derivatives are converted to *gem*-difluorides using Deoxo-Fluor, see: Lal, G. S.; Lobach, E.; Evans, A. Fluorination of thiocarbonyl compounds with bis(2-methoxythyl)aminosulfur trifluoride (Deoxo-Fluor Reagent): A facile synthesis of *gem*-difluorides. *J. Org. Chem.* **2000**, *65*, 4830−4832.
(33) The direct boronic acid catalyzed dimerization approach used to prepare diketopiperazine **1** was not optimal for use with *trans*-C4-fluoro-L-proline due to poor solubility.
(34) Nicolaou, K. C.; Giguère, D.; Totokotsòpoulos, S.; Sun, Y.-P. A practical sulfenylation of 2,5-diketopiperazines. *Angew. Chem., Int. Ed.* **2012**, *51*, 728−732.
(35) Boyer, N.; Movassaghi, M. Concise total synthesis of (+)-gliocladins B and C. *Chem. Sci.* **2012**, *3*, 1798−1803.
(36) (a) Choudhary, A.; Gandla, D.; Krow, G. R.; Raines, R. T. Nature of amide carbonyl−carbonyl interactions in proteins. *J. Am. Chem. Soc.* **2009**, *131*, 7244−7246. (b) Choudhary, A.; Raines, R. T. Signature of $n\rightarrow\pi^*$ interactions in α-helices. *Protein Sci.* **2011**, *20*, 1077−1081. (c) Choudhary, A.; Kamer, K. J.; Raines, R. T. An $n\rightarrow\pi^*$ interaction in aspirin: Implications for structure and reactivity. *J. Org. Chem.* **2011**, *76*, 7933−7937. (d) Kamer, K. J.; Choudhary, A.; Raines, R. T. Intimate interactions with carbonyl groups: Dipole-dipole or $n\rightarrow\pi^*$? *J. Org. Chem.* **2013**, *78*, 2099−2103. (e) Newberry, R. W.; Raines, R. T. $n\rightarrow\pi^*$ Interactions in poly(lactic acid) suggest a role in protein folding. *Chem. Commun.* **2013**, *49*, 7699−7701. (f) Newberry, R. W.; VanVeller, B.; Guzei, I. A.; Raines, R. T. $n\rightarrow\pi^*$ Interactions of amides and thioamides: Implications for protein stability. *J. Am. Chem. Soc.* **2013**, *135*, 7843−7846. (g) Choudhary, A.; Fry, C. G.; Kamer, K. J.; Raines, R. T. An $n\rightarrow\pi^*$ interaction reduces the electrophilicity of the acceptor carbonyl group. *Chem. Commun.* **2013**, *49*, 8166−8168. (h) Guzei, I. A.; Choudhary, A.; Raines, R. T. Pyramidalization of a carbonyl C atom in (2*S*)-*N*-(selenoacetyl)-proline methyl ester. *Acta Crystallogr., Sect. E: Struct. Rep. Online* **2013**, *69*, o805−o806. (i) Newberry, R. W.; Bartlett, G. J.; VanVeller, B.; Woolfson, D. N.; Raines, R. T. Signatures of $n\rightarrow\pi^*$ interactions in proteins. *Protein Sci.* **2014**, *23*, 284−288. (j) Newberry, R. W.; Raines, R. T. A key $n\rightarrow\pi^*$ interaction in *N*-acyl homoserine lactones. *ACS Chem. Biol.* **2014**, *9*, 880−883. (k) Choudhary, A.; Newberry, R. W.; Raines, R. T. $n\rightarrow\pi^*$ Interactions engender chirality in carbonyl groups. *Org. Lett.* **2014**, *16*, 3421−3423. (l) Wilhelm, P.; Lewandowski, B.; Trapp, N.; Wennemers, H. A crystal structure of an oligoproline PPII-helix, at last. *J. Am. Chem. Soc.* **2014**, *136*, 15829−15832. (m) Newberry, R. W.; Raines, R. T. Crystal structure of *N*-(3-oxobutanoyl)-L-homoserine lactone. *Acta Crystallogr., Sect. E: Struct. Rep. Online* **2016**, *72*, 136−139. (n) Rahim, A.; Sahariah, B.; Sarma, B. K. *N*,*N*′-Di(acylamino)-2,5-diketopiperazines: Strategic incorporation of reciprocal $n\rightarrow\pi^*$ Interactions in a druglike scaffold. *Org. Lett.* **2018**, *20*, 5743−5746.
(37) Because of systematic spectral overlap, these values are upper limits. The actual values of $E^{\circ\prime}$ could be <30 mV lower, that is, more negative.
(38) Lees, W. J.; Whitesides, G. M. Equilibrium constants for thiol-disulfide interchange reactions: A coherent, corrected set. *J. Org. Chem.* **1993**, *58*, 642−647.
(39) Winkler, F. K.; Dunitz, J. D. The non-planar amide group. *J. Mol. Biol.* **1971**, *59*, 169−182.
(40) (a) Birk, J.; Meyer, M.; Aller, I.; Hansen, H. G.; Odermatt, A.; Dick, T. P.; Meyer, A. J.; Appenzeller-Herzog, C. Endoplasmic reticulum: Reduced and oxidized glutathione revisited. *J. Cell Sci.* **2013**, *126*, 1604−1617. (b) Schwarzländer, M.; Dick, T. P.; Meyer, A. J.; Morgan, B. Dissecting redox biology using fluorescent protein sensors. *Antioxid. Redox Signaling* **2016**, *24*, 680−712.
(41) (a) Ostergaard, H.; Tachibana, C.; Winther, J. R. Monitoring disulfide bond formation in the eukaryotic cytosol. *J. Cell Biol.* **2004**, *166*, 337−345. (b) Morgan, B.; Ezerina, D.; Amoako, T. N.; Riemer, J.; Seedorf, M.; Dick, T. P. Multiple glutathione disulfide removal pathways mediate cytosolic redox homeostasis. *Nat. Chem. Biol.* **2013**, *9*, 119−125.
(42) (a) Shoulders, M. D.; Kotch, F. W.; Choudhary, A.; Guzei, I. A.; Raines, R. T. The aberrance of the 4*S* diastereomer of 4-hydroxyproline. *J. Am. Chem. Soc.* **2010**, *132*, 10857−10865. (b) Erdmann, R. S.; Wennemers, H. Importance of ring puckering versus interstrand hydrogen bonds for the conformational stability of collagen. *Angew. Chem., Int. Ed.* **2011**, *50*, 6835−6838. (c) Erdmann, R. S.; Wennemers, H. Effect of sterically demanding substituents on the conformational stability of the collagen triple helix. *J. Am. Chem. Soc.* **2012**, *134*, 17117−17124. (d) Siebler, C.; Erdmann, R. S.; Wennemers, H. Switchable proline derivatives: Tuning the conformational stability of the collagen triple helix by pH changes. *Angew. Chem., Int. Ed.* **2014**, *53*, 10340−10344.

https://dx.doi.org/10.1021/jacs.0c06477
J. Am. Chem. Soc. 2020, 142, 15107−15115